

Design, analyses, and evaluation of a spiral TDR sensor with high spatial resolution

Quan Gao^{1a}, Guangxi Wu^{2b} and Xiong Yu^{*1}

¹Department of Civil Engineering, Case Western Reserve University, Cleveland, OH, USA

²Department of Electrical Engineering and Computer Science, Case Western Reserve University, Cleveland, OH, USA

(Received November 6, 2014, Revised April 29, 2015, Accepted April 30, 2015)

Abstract. Time Domain Reflectometry (TDR) has been extensively applied for various laboratory and field studies. Numerous different TDR probes are currently available for measuring soil moisture content and detecting interfaces (i.e., due to landslides or structural failure). This paper describes the development of an innovative spiral-shaped TDR probe that features much higher sensitivity and resolution in detecting interfaces than existing ones. Finite element method (FEM) simulations were conducted to assist the optimization of sensor design. The influence of factors such as wire interval spacing and wire diameter on the sensitivity of the spiral TDR probe were analyzed. A spiral TDR probe was fabricated based on the results of computer-assisted design. A laboratory experimental program was implemented to evaluate its performance. The results show that the spiral TDR sensor featured excellent performance in accurately detecting thin water level variations with high resolution, to the thickness as small as 0.06 cm. Compared with conventional straight TDR probe, the spiral TDR probe has 8 times the resolution in detecting the water level changes. It also achieved 3 times the sensitivity of straight TDR probe.

Keywords: time domain reflectometry; TDR; spiral TDR probe; sensor; interface detection; computer-aid design

1. Introduction

Time Domain Reflectometry (TDR) is an electromagnetic geophysical technique that measures material properties by use of the propagation speed and attenuation of electromagnetic (EM) wave. It was originally employed to locate discontinuities in electrical cable (Benson and Bosscher 1999). Over the past decades, it has been extensively used for civil and environmental applications, including characterization of soils and concrete (Drnevich *et al.* 2001, Hager III and Domszy 2004, Noborio 2001, O'Connor and Dowding 1999, Topp and Davis 1985, Yu and Drnevich 2004), monitoring infrastructure conditions (Chen *et al.* 2004, Lin *et al.* 2005, Su and Chen 1998), contaminants transportation (Haridy *et al.* 2004), detecting freeze/thaw behaviors of soils (Liu *et*

*Corresponding author, Associate Professor, E-mail: xxy21@case.edu

^a Ph.D. Candidate, E-mail: qyg29@case.edu

^b Ph.D. Candidate, E-mail: gwx94@case.edu

al. 2012) and monitoring seepage processes in embankment (Bin *et al.* 2010), etc.

Various types of TDR probes were designed and utilized for different applications, such as two/three-rod straight probe (Siddiqui and Drnevich 1995), strip probe (Bin *et al.* 2010), serpentine probe (Selker *et al.* 1993), and coaxial-type probe (White and Zegelin 1994), etc. Some of these TDR sensors can achieve resolution within centimeter range for interface detections. However, certain applications require detection of interfaces with much higher resolution. TDR probe with spiral-shape was found to be a potential means to achieve this goal (Bittelli *et al.* 2004, Katsura *et al.* 2008, Lungal and Si 2008, Nissen *et al.* 1998, Vaz and Hopmans 2001). Nissen *et al.* (1998) presented a coiled TDR probe to improve the resolution of TDR sensor. In this design, one rod of the TDR probe was made in spiral shape while the other one as straight. Vaz and Hopmans (2001) combined coiled TDR probe with a penetrometer to measure the soil water content and penetration resistance simultaneously. Katsura *et al.* (2008) utilized coil-type TDR probe in a field monitoring program on the long term evolution of water content in weathered granitic bedrock. The stainless wires were closely coiled without gap between the adjacent wires, which would lead to retention of moisture and compromise its capability in real time detection of wetting and drying processes. Lungal and Si (2008) designed a TDR probe with dual-threaded Plexiglas core instead of smooth rod. The design made it easy to control the interval space. However, the unthreaded part between two adjacent threads compromised the measurement accuracy.

This paper introduces the design and assessment of a new spiral TDR probe that features high spatial resolution while resolving the problems described in the previous context. It firstly provides an overview on the background of TDR technology and principles for TDR probe design (i.e., the effective sampling area of TDR probe). Finite Element Method (FEM) simulation was conducted to analyze the influence of probe design parameters (i.e., interval between spiral wire waveguide and dimension of the spiral wire) on the effective sampling area of the spiral TDR probe. Based on the effective sampling area and manufacturability considerations, the design of spiral TDR sensor was optimized. A new spiral TDR sensor is fabricated based on the computation assisted design analyses. A special coating treatment using super-hydrophobic coating was applied to prevent the intraptraption of water and the consequent hysteresis in sensor responses. The performance of the new TDR spiral probe was evaluated in laboratory experiments. The results showed that the sensor achieved significantly higher spatial resolution for interface detection than conventional TDR sensors.

2. Principle of time domain reflectometry

A schematic of a typical TDR system is shown in Fig. 1(a), which includes a TDR pulse generator, coaxial cable, a TDR probe, and control computer (a datalogger, laptop or PDA). The TDR pulse generator produces a fast rising electrical pulse (with rising time of picoseconds by state-of-art electronics) that propagates along the coaxial cable to the TDR sensor probe. The sensor probe is embedded and surrounded by materials under investigation (e.g., soil, concrete). When the EM wave associated with the electrical pulse reaches the surface of soil, a portion of signal is reflected back due to the impedance mismatch between air and soil, whereas the rest of wave continues to travel to the end of probe where it is subjected to complete reflection. This results in two distinctive reflections as the footprint in the TDR signal (i.e., Fig. 1(b)). The distance or time lapse between the two reflections is related to the speed of EM wave in the material.

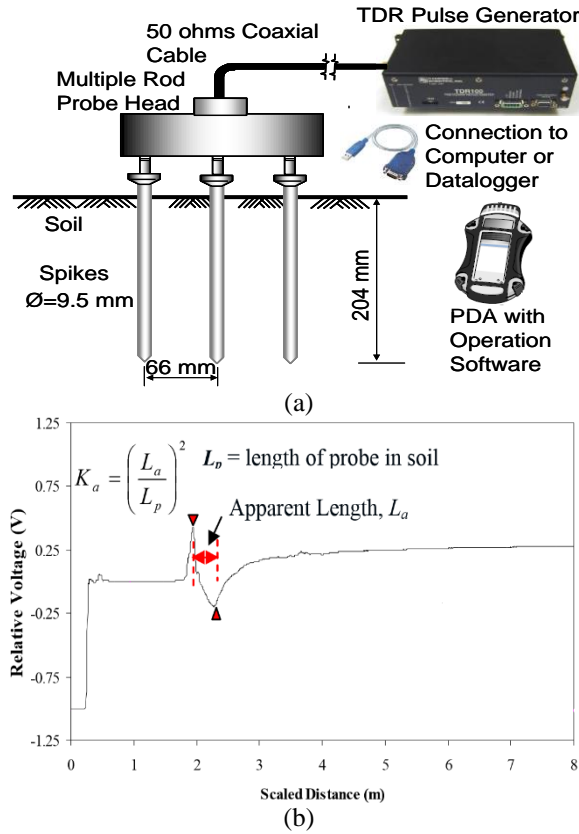


Fig. 1 (a) Schematic diagram of a TDR system and (b) A typical TDR signal

The velocity, v , of electromagnetic wave through a material is related to its dielectric constant, K_a , as following

$$v = \frac{c}{\sqrt{K_a}} \tag{1}$$

Where c is the velocity of an EM wave in free space $2.998 \times 10^8 m/s$; K_a is the apparent dielectric constant of the material. Assuming the embedded length of TDR probe is L_p , the time required for EM wave to round trip through the probe can be calculated by Eq. (2).

$$t = \frac{2L_p}{v} \tag{2}$$

Substituting Eqs. (1) into (2) and defining apparent length, $L_a=ct/2$, there is

$$K_a = \left(\frac{L_a}{L_p}\right)^2 \tag{3}$$

where the apparent length, L_a , is the distance between two reflections in TDR signal, which can be directly obtained from Fig. 1(b).

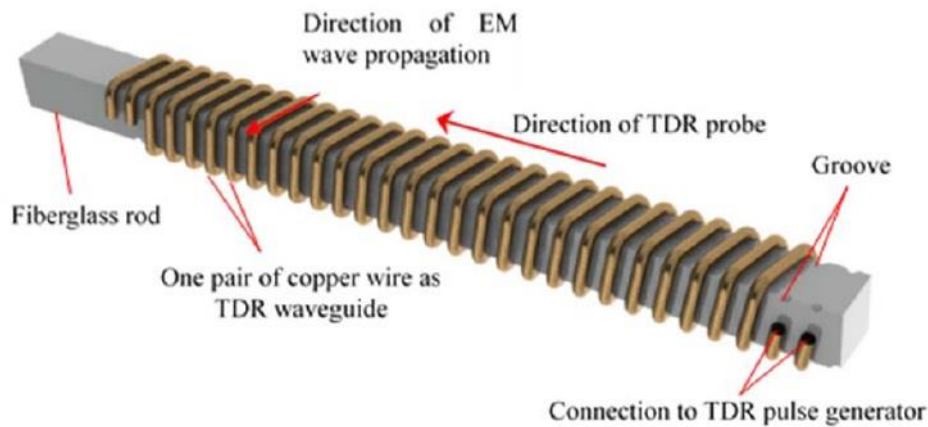


Fig. 2 Schematic of working principles of spiral TDR sensor

3. Motivation for new TDR sensor development

A number of applications involve the detection of interfaces. Conventional TDR probe are mostly based on straight metallic rods. This together with the frequency of TDR EM waves possesses a constraint on the resolution of common types of TDR sensor in detecting the interface. Traditional TDR sensors detect interfaces at resolution in the centimeter range for typical applications. To further improve the resolution, an innovative spiral TDR sensor design is pursued in this paper. The basic idea of a spiral TDR probe design is that with a spiral propagation path, the effective travelling distance per unit length along the direction of the sensor probe is increased (Fig. 2). This, therefore, will lead to improvements of the resolution of the sensor in detecting the interface.

4. Computer-aid design of spiral TDR probe

Factors determining the performance of a spiral TDR probe include the properties of the sensor wire (i.e., diameter) and the spatial arrangement (spiral angle and wire spacing). Computational simulations are implemented to assist the optimization design of the spiral TDR probe. The technical background of computational assisted TDR probe design simulations is summarized in the following sections.

4.1 Electrical field distribution around a TDR probe

The dominant mode of EM wave in a TDR waveguide is the Transverse Electromagnetic (TEM) wave mode. In the cross section perpendicular to the direction of EM wave propagation, the electric field of TDR probes can be treated as an electrostatic problem and the electrostatic potential satisfies Poisson's equation (Ferré *et al.* 1998, Knight *et al.* 1997, Yu and Yu 2009), i.e., Eq. (4).

$$\nabla \cdot (\epsilon \nabla V) = -\rho \tag{4}$$

where ϵ is the permittivity of the medium; ρ is the space charge density, which are both a function of space coordinate; V is the electrical potential. The charge density can be assumed as zero for typical dielectric material (Bin *et al.* 2010, Yu and Yu 2009).

The Poisson’s equation must be solved with finite element method due to highly nonlinearity. From the results, information such as the electrical potential field distribution and the electrical energy density can be determined.

4.2 Effective sampling and sensing area of TDR probes

The electrical energy density distribution is used to determine the effective sampling area of spiral TDR probe. The spatial sampling area is associated with the spatial sensitivity of TDR probes (Ferré *et al.* 1998, Ferré *et al.* 2000, Ferré *et al.* 1996, Knight 1992, Knight *et al.* 1997, Nissen *et al.* 2003, Yu 2009).

The effective sampling area of TDR probe in the plane perpendicular to the TDR probe is defined as the region that contributes to the total probe response (Ferré *et al.* 1998). The influence of materials outside this area can be neglected without causing significant error. To determine the effective sampling area, spatial weighting function are employed to consider the spatial contributions to the overall electrical field (Nissen *et al.* 2003).

Ferré *et al.* (1998) presented a numerical method to determine the effective sampling area of TDR probe based on the spatial weighting function. As shown in Eq. (5), starting from the element with the highest weighting function value, the product of weighting function and the area of the element is summed until its cumulative value equals to a certain fraction (e.g., 90%) of the integration value over the whole domain.

$$f = \frac{100 \cdot \sum w_{hi} w_i A_i}{\iint_{\Omega} w_i dA} \tag{5}$$

where w_i denotes the spatial weighting function; A_i denotes the element area; w_{hi} denotes the highest weighting function.

For the contribution to the electrical field, the weighting function, w_i , is replaced with the electric energy density, w_{ei} (Yu and Yu 2009). Therefore, the sampling area of TDR probe can be determined from Eq. (6).

$$f = \frac{100 \cdot \sum w_{hi} w_{ei} A_i}{\iint_{\Omega} w_{ei} dA} \tag{6}$$

in which, w_{ei} is the electric energy density, which can be acquired from the solution of Eq. (4); f is the percent contribution to the total weighted average values. In this study, 90% sampling area is selected to demonstrate the numerical simulation results.

4.3 Implementation of computational simulations

Direct simulation of the electrostatic potential distribution of a spiral TDR probe (Fig. 2) requires solving three-dimensional Maxwell’s equations. To simplify the analyses while not causing too much error, a 2D approximation is used to study the design of spiral TDR wires (Ferré *et al.* 1998). A two dimensional model of the longitudinal section of spiral probe is constructed in

this study (Fig. 3). Due to the symmetry of the wire probe, half of the cross section was considered, where D denotes the diameter of the copper wire; d denotes the interval space between adjacent wires; L denotes the side length of the central rod; and S denotes the center distance of adjacent two pairs of electrodes (center-center distance of two positive-negative electrodes), $S = 2(D + d)$.

A general FEM software, COMSOL Multiphysics®, was utilized to solve Poisson's equation (Eq. (4)) for the spiral probe. Fig. 4 shows the mesh grid of the computation domain. The computational domain was selected to be sufficiently large so that further increase in the size of the domain does not have significant influence on the electrical field distribution. The rectangle represents the fiberglass rod where the TDR waveguide wires are mounted. The circles represent the pair of copper wires that acts as positive and negative electrodes, respectively. The copper wire was assumed to be covered with one layer of insulation coating with thickness of 0.5 mm. The dielectric constant was set as 3.5 according to the properties of coating material. The sensor was assumed to be inundated in water, whose dielectric constant was set as 81. The dielectric constant of fiberglass was set as 5.0. The unit potential of +1 V and -1 V were set for the two electrodes. The value of the potential only affects the magnitude of the electrical field and has no effect on the distribution pattern of the electric field (Knight *et al.* 1997, Yu 2009).

Factors including the diameter of the wire, D , and space between two adjacent wires, d , were taken into account in the simulation analysis (Table 1).

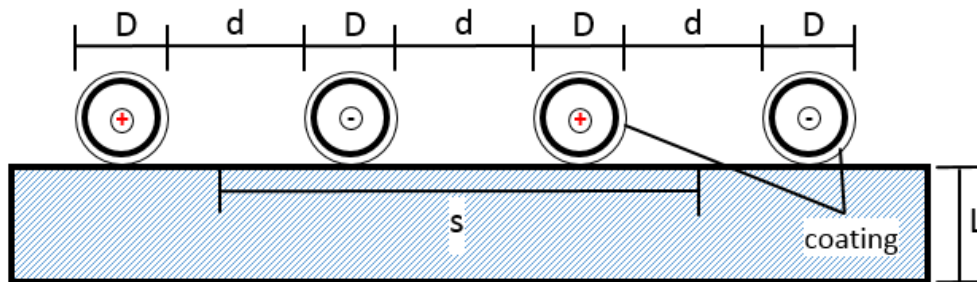


Fig. 3 Schematic diagram of spiral probe for FEM analysis

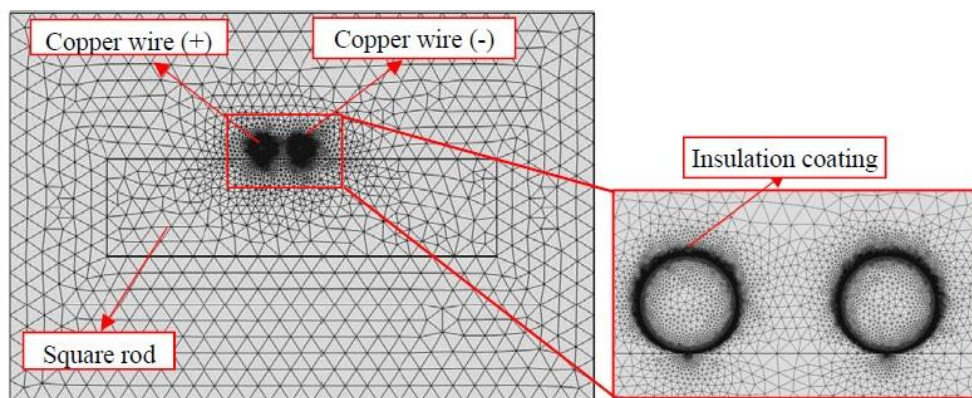


Fig. 4 Mesh grid of computation domain

Table 1 Configurations of simulation parameters

Distance, d (mm)	Diameter, D (mm)
0, 1, 2, 3, 4, 5	1, 2, 3, 4, 5

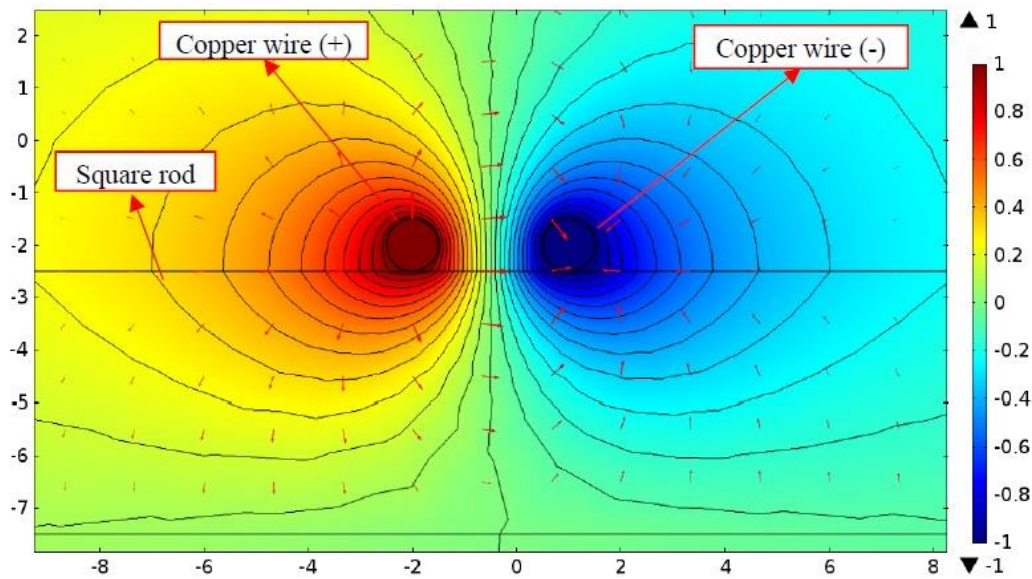


Fig. 5 Electric potential (contour and color, unit: Volt) and electric field (red arrow) distribution (in water) (length unit: mm)

4.4 Simulation Results and Analysis

4.4.1 Electrostatic field distribution

Fig. 5 and Fig. 6 show the electric potential and electric energy density distribution respectively when the sensor is submerged in water. In Fig. 5, the isolines of electrical potentials are circles centered at both electrodes and symmetric. There is a knee point for each potential isoline at the interface of fiberglass rod and water due to contrast in dielectric constant. From Fig. 6, the effective sampling area contributing 90% of the total electric field energy were determined to be $2.71 \times 10^{-5} m^2$ using the Eq. (6). The domain with higher values of dielectric constant (water) has larger energy density than that with lower values of dielectric constant (fiberglass core rod), which is consistent with observations in other studies (Knight *et al.* 1997, Yu 2009).

4.4.2 Effect of wire distance on sampling area

The influence of wire distance, d , on sampling area (90% of total electrical energy) is illustrated in Fig. 7, while the diameter of wire is set as 1 mm. There is a linear relationship between effective sampling area and wire spacing. This is consistent with the characteristics of conventional

two/three rod probe given by Ferré *et al.* (2001) and Nissen *et al.* (2003). Therefore, design with larger wire spacing is able to improve effective sampling area of the sensor.

However, the larger wire spacing will reduce the resolution of the spiral probe (Fagert *et al.* 2014). Also, it could cause potential overlap of sampling area in the adjacent spiral wire pairs. To improve and optimize the sampling efficiency of the probe, Eq. (7) can be utilized as the criteria of wire spacing, in which d and S have the same meaning as that illustrated in Fig. 3, and l is assumed to be length of long axis of 90% sampling area in Fig. 6.

$$l \leq 2(D + d) \tag{7}$$

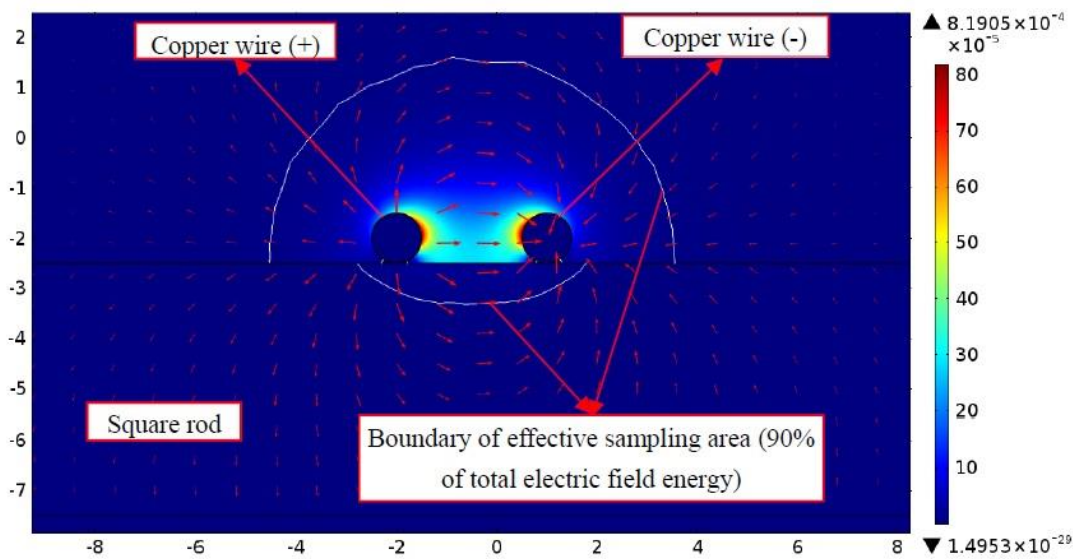


Fig. 6 Electric energy density (color, unit: volt), effective sampling area with 90% level (contour) and electric field (red arrow) distribution (filled in water) (length unit: mm)

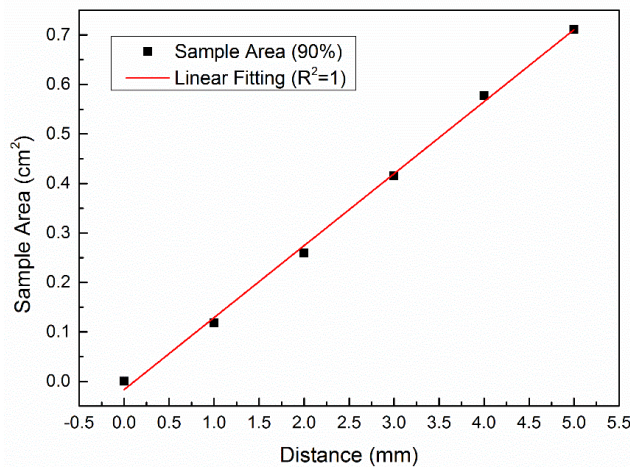


Fig. 7 Influence of wire distance on sample area

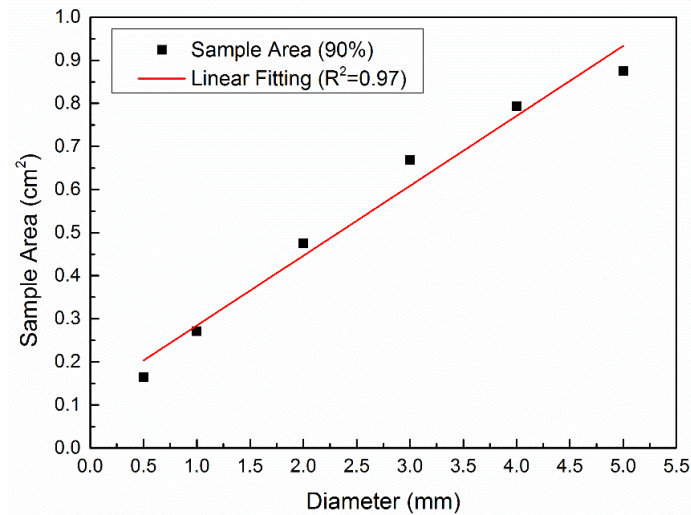


Fig. 8 Influence of wire diameter on sample area

4.4.3 Effect of wire diameter on sample area

Fig. 8 illustrates the influence of wire diameter on effective sampling area when the distance between adjacent wires is set as 2 mm. The sampling area increases linearly with the wire diameter. However, it is impossible to manufacture a coil TDR sensor with too large diameter due to practical limitations, even though the effective sampling area increases significantly.

5. Design and fabrication of spiral sensor

Proper spiral probe parameters (i.e., wire diameter, wire spacing, mounting materials, etc) should be chosen by considering factors such as the effective sampling area, manufacturability, and application requirements. Based on a comprehensive evaluation of the design parameters, copper conductive wire with diameter of 1 mm was selected to make spiral TDR sensor; the spacing between the wires was set as 2 mm; and the mounting rod is chosen as square fiberglass rod with 5 mm in side length and 250 mm in length. Photo of the sensor is shown in Fig. 9. The inclination angle of the wire around center rod is about 22° , which could effectively prevent retention of water between two adjacent wires. Fabrication grooves were created along the fiberglass rod to facilitate the control of wire spacing. Note grooves were only carved at the corner of the square rod to avoid the measurement influence similar to Lungal and Si (2008). Two copper conductive wires are wrapped in parallel around the fiberglass rod with predefined spacing. The copper wires are coated by polyurethane, a widely used commercial insulation material.

In order to eliminate the lagging effects of spiral sensor due to residual water between two adjacent wires when water level retreats, a commercial superhydrophobic coating is sprayed to completely cover the surface of the rod. The effects of this superhydrophobic coating on the performance of new spiral probe will be evaluated and discussed in the subsequent section of this paper.



Fig. 9 Photo of spiral-shaped TDR probe

The spiral probe made for this study is 25 cm long, which can be adjusted for a specific application. At the end of the spiral wire, an adapter is used to connect the coaxial cable and TDR system.

6. Evaluation of spiral TDR sensor

Laboratory experiments were conducted to evaluate the performance of the spiral probe. Three TDR sensors with identical equivalent length are prepared (Fig. 9), including (1) conventional straight probe, (2) spiral probe without superhydrophobic coatings, and (3) spiral probe with coatings. The texture and fabrication of the three sensors are identical. The traditional two rod probe (sensor 1) is used as a control group. Sensor 3 is treated by spraying a layer of superhydrophobic coating.

6.1 Comparison with traditional two rod TDR probe

Straight and spiral probes (sensor 1 and sensor 3) were firstly tested in air and water. Fig. 10 shows the output signals of two sensors. The black arrows in both figures represent reflection points of EM wave at air-water interface and probe end, which are determined using tangential line method (Yu and Drnevich 2004). The apparent length for each case are acquired by following the previous section of this study, which are listed in Table 2.

From both Fig. 10 and Table 2, for the same probe length, the apparent length of spiral probe is much larger than that of two-rod straight probe, i.e., around $1.285/0.241=7.7$ and $5.181/1.405=3.7$ times of in air and water, respectively. This indicates that the resolution of TDR sensor can be significantly improved by spiral design. The extent of improvement, however, is associated with the dielectric permittivities of material around the probe.

Table 2 Comparison of apparent length of two sensors in air and water

Sensor type	Starting point (m)	Ending point (m)	Scaled length (m)	Note
Straight probe	7.189	7.430	0.241	Air
Spiral probe	7.189	8.474	1.285	
Straight probe	7.209	8.614	1.405	Water
Spiral probe	7.209	12.39	5.181	

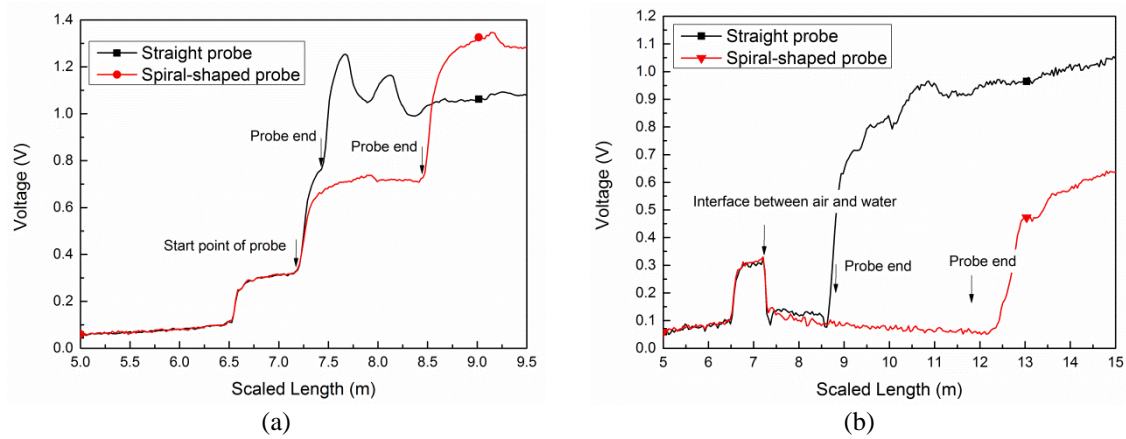


Fig. 10 Comparison of traditional and spiral TDR probe ((a)- in the air and (b)- totally submerged in the water)

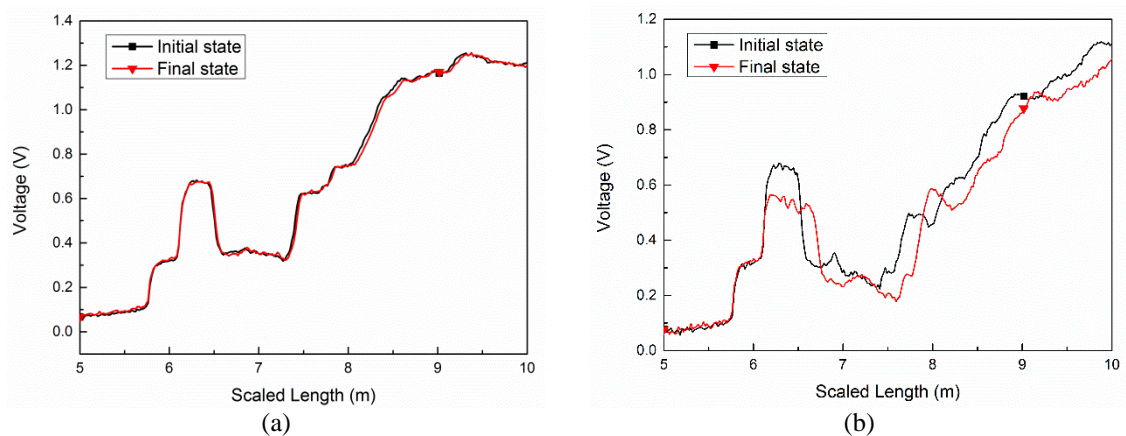


Fig. 11 Comparison of spiral TDR probe with and without superhydrophobic coating ((a)- with coating and (b)- without coating)

6.2 Effect of superhydrophobic coating

The spiral geometry might potentially allow water to be trapped between the adjacent spiral wires. Superhydrophobic coating was applied to prevent this phenomena. To evaluate the effect of superhydrophobic coating on the performance of spiral TDR probe, sensor 2 and sensor 3 were tested in the tank full with water.

The test procedures include the following steps: 1) two sensors were partially submerged into a plastic tank with 30 cm of water; a TDR signal is acquired and named as “initial state”; 2) water was added into the tank to totally submerge the two TDR sensors; 3) the depth of tap water was then decreased to the “initial state”, and a second TDR signal was acquired and named as “final state”.

Fig. 11 shows the output signals of the two sensors at the initial and final state. As illustrated in Fig 11(b), spiral probe without coating treatment shows hysteresis behavior due to trapping of water along the wire probe. The spiral probe with superhydrophobic coating (Fig. 11(a)), however, shows excellent repeatability that is not affected by cyclic water level variation or fluctuation. This implies that the superhydrophobic coating was effective in preventing water residing on the spiral wires.

6.3 Sensitivity of spiral TDR probe

Experiments were also conducted in a plastic tank with 25 cm of water column to assess the sensitivity of the spiral probe. A modified micrometer is employed to control and measure the depth of sensor submerged in water with an accuracy of 0.01 mm. As shown in Fig. 12, TDR probes (sensor 1 and sensor 3) were fixed at the end of micrometer and then gradually dipped into water each 0.025 inch (around 0.06 mm) by adjusting micrometer.

Fig. 13 shows the acquired TDR signal at different water levels for both straight and spiral probe (sensor 1 and sensor 3). The initial state is denoted as “25 cm” and the signal at arbitrary state is written as “25 cm + x mm”, x means the additional depth of sensors submerged into water. For example, “25 cm+0.06 mm” means the sensor is dipped into water by 0.06 mm more. This process is continued to the state of “25 cm + 1.5 cm”. Figs. 13(a) and 13(b) illustrate the output signals of two sensors for water level variation by 0.06 cm, while Figs. 13(c) and 13(d) show that when water level varies every 0.5 cm.

From Figs. 13(a) and 13(b), no obvious change can be observed for the output signals of traditional two-rod probe, however, the reflection point at the probe end offsets significantly for the spiral probe. This indicates that the spiral TDR probe is sufficiently sensitive to detect a 0.06 cm change in water layer, compared to that of straight probe in Fig. 13(c) (0.5 cm). This means the resolution of spiral sensor in this study is around $0.5/0.06 = 8$ times of two rod straight probe to detect the variation of water level.

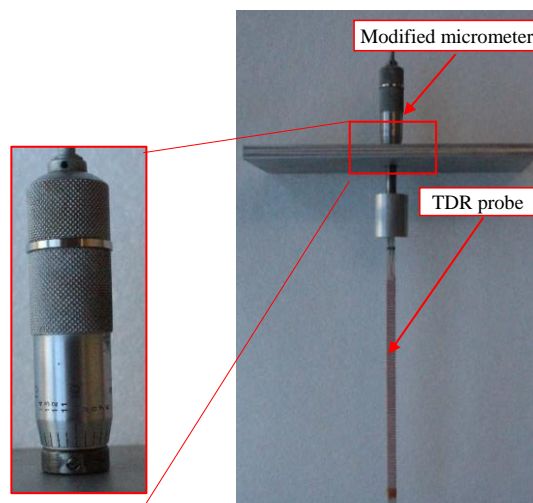
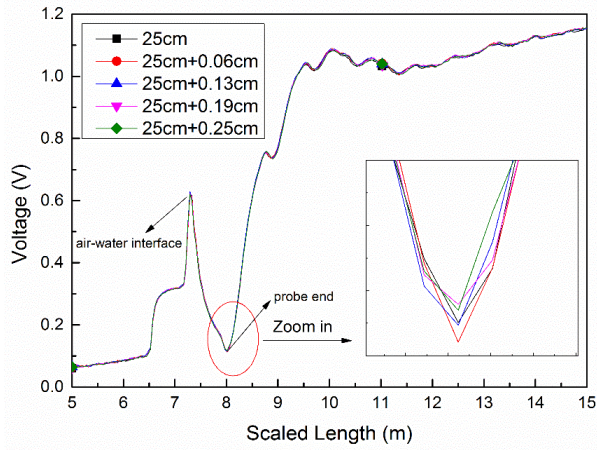
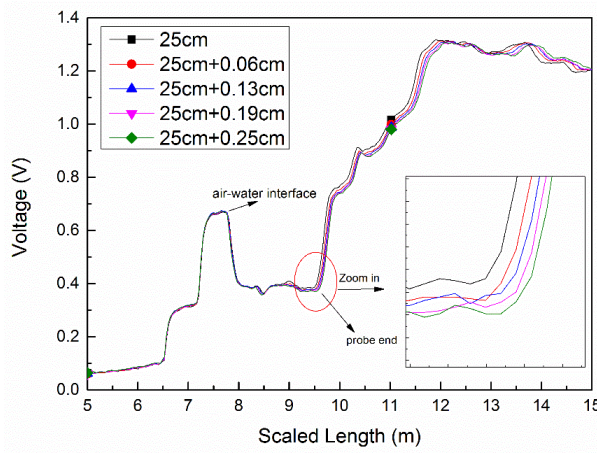


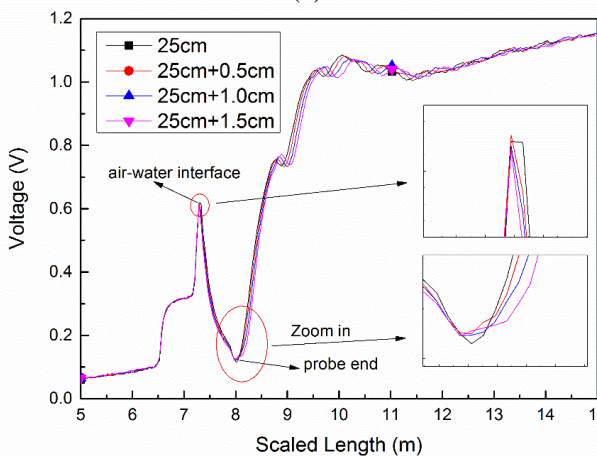
Fig. 12 Photo of converted micrometer



(a)



(b)



(c)

Continued-

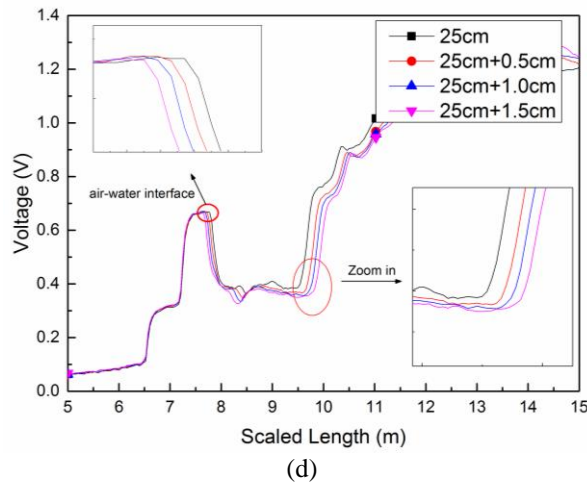


Fig. 13 Output signals of two-rod straight and spiral probe at different water levels ((a), (c)-straight probe; (b), (d)- spiral probe)

Figs. 13(c) and 13(d) show the output signals of two sensors when water level varies every 0.5 cm. Both probes demonstrate an apparent offset at the reflection point of probe end. However, only signal from spiral probe has appreciable offsets at the reflection point of the air-water interface. The signal of the straight probe does not respond obviously. Change of air layer as think as 0.5 cm causes much more appreciable change in the signals by the spiral TDR probe compared with straight TDR probe.

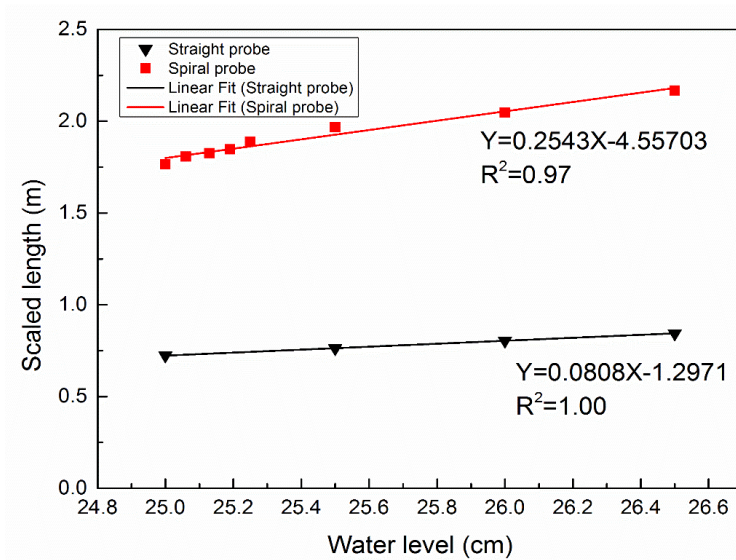


Fig. 14 Relationship between scaled length and water level (air-water interface) for two sensors

Fig. 14 shows the relationship between scaled length and water levels measured by straight and spiral TDR sensor. In terms of linear curve-fitting equations in Fig. 14, the sensitivity of both sensors to detect water layer are 0.08 and 0.25, respectively, which means the spiral TDR probe is around 3 times more sensitive than a straight TDR probe. The spiral TDR probe shows slight non-linear responses, which is possibly due to the fabrication issues. It is expected that the sensitivity and linearity of the spiral TDR probe can be further improved refining the design and fabrication procedures.

7. Conclusions

This paper presents the design, fabrication and evaluation of an innovative spiral TDR sensor that improves the resolution and sensitivity in interface detection. FEM simulations were conducted to determine the effective sampling area and assist the design of spiral TDR sensor. From the results, sensor geometry (i.e., wire interval spacing, wire diameter) on the effective sampling area of the spiral TDR probe is determined. The performance of this new sensor is evaluated in laboratory experiments. The results indicate that the spiral TDR sensor achieved much higher resolution in detecting the air-water interface. The spatial resolution of the spiral TDR sensor in detecting water level variation is at least 8 times higher than that of conventional straight TDR probe. The spiral probe has about 3 times the sensitivity of the straight TDR probe to detect water level changes.

Acknowledgements

We acknowledge the support of Saada Family fellowship in the course of this study. This study is also partially supported by the U.S. National Science Foundation (Grant No. 0900401, 1131295). The assistance from Jim Berilla, department technician, is also highly appreciated.

References

- Benson, C.H., and Bosscher, P.J. (1999), "Time-domain reflectometry (TDR) in geotechnics: a review", *Nondestructive and Automated Testing for Soil and Rock Properties*, ASTM STP, 1350, 113-136.
- Bin, Z., Xinbao, Y. and Xiong, Y. (2010), "Design and evaluation of a distributed TDR moisture sensor", *Smart Struct. Sys.*, **6**(9), 1007-1023.
- Bittelli, M., Flury, M., Campbell, G.S. and Schulz, V. (2004), "Characterization of a spiral-shaped time domain reflectometry probe", *Water Resour Res.*, **40**(9).
- Chen, G., Mu, H., Pommerenke, D. and Drewniak, J.L. (2004), "Damage detection of reinforced concrete beams with novel distributed crack/strain sensors", *Struct. Health Monit.*, **3**(3), 225-243.
- Drnevich, V.P., Siddiqui, S.I., Lovell, J. and Yi, Q. (2001), "Water content and density of soil insitu by the purdue TDR method", *Proceedings of the 2nd International Symposium on Time Domain Reflectometry*.
- Fagert, J., Zhang, B., Gao, Q. and Yu, X.B. (2014), *Sensor for detection of earthquake induced void redistribution in multi-layered soil system*.
- Ferré, P., Knight, J., Rudolph, D. and Kachanoski, R. (1998), "The sample areas of conventional and alternative time domain reflectometry probes", *Water Resour Res.*, **34**(11), 2971-2979.
- Ferré, P., Knight, J., Rudolph, D. and Kachanoski, R. (2000), "A numerically based analysis of the

- sensitivity of conventional and alternative time domain reflectometry probes”, *Water Resour Res.*, **36**(9), 2461-2468.
- Ferré, P., Rudolph, D. and Kachanoski, R. (1996), “Spatial averaging of water content by time domain reflectometry: Implications for twin rod probes with and without dielectric coatings”, *Water Resour Res.*, **32**(2), 271-279.
- Ferré, P.A., Nissen, H.H., Moldrup, P. and Knight, J.H. (2001), “The sample area of time domain reflectometry probes in proximity to sharp dielectric permittivity boundaries”, *Proceedings of the TDR 2001 2nd International Symposium and Workshop on Time Domain Reflectometry for Innovative Geotechnical Applications*, Infrastructure Technology Institute, Northwestern University, Evanston, IL.
- Hager III, N. and Domszy, R. (2004), “Monitoring of cement hydration by broadband time-domain-reflectometry dielectric spectroscopy”, *J. Appl. Phys.*, **96**(9), 5117-5128.
- Haridy, S.A., Persson, M. and Berndtsson, R. (2004), “Estimation of LNAPL saturation in fine sand using time-domain reflectometry/Estimation de la saturation en LPNAL dans du sable fin grâce à la réflectométrie en domaine temporel”, *Hydrolog. Sci. J.*, **49**(6).
- Katsura, S.Y., Kosugi, K.I. and Mizuyama, T. (2008), “Application of a coil-type TDR probe for measuring the volumetric water content in weathered granitic bedrock”, *Hydrol Process.*, **22**(6), 750-763.
- Knight, J. (1992), “Sensitivity of time domain reflectometry measurements to lateral variations in soil water content”, *Water Resour Res.*, **28**(9), 2345-2352.
- Knight, J., Ferré, P., Rudolph, D. and Kachanoski, R. (1997), “A numerical analysis of the effects of coatings and gaps upon relative dielectric permittivity measurement with time domain reflectometry”, *Water Resour Res.*, **33**(6), 1455-1460.
- Lin, M.W., Thaduri, J. and Abatan, A.O. (2005), “Development of an electrical time domain reflectometry (ETDR) distributed strain sensor”, *Measurement Sci. Technol.*, **16**(7), 1495.
- Liu, Z., Yu, X., Yu, X. and Gonzalez, J. (2012), “Time domain reflectometry sensor-assisted freeze/thaw analysis in geomaterials”, *Cold Reg. Sci. Technol.*, **71**, 84-89.
- Lungal, M. and Si, B.C. (2008), “Coiled time domain reflectometry matric potential sensor”, *Soil. Sci. Soc. Am. J.*, **72**(5), 1422-1424.
- Nissen, H.H., Ferré, T. and Moldrup, P. (2003), “Sample area of two-and three-rod time domain reflectometry probes”, *Water Resour Res.*, **39**(10).
- Nissen, H.H., Moldrup, P. and Henriksen, K. (1998), “High-resolution time domain reflectometry coil probe for measuring soil water content”, *Soil. Sci. Soc. Am. J.*, **62**(5), 1203-1211.
- Noborio, K. (2001), “Measurement of soil water content and electrical conductivity by time domain reflectometry: a review”, *Comput. Electron. Agr.*, **31**(3), 213-237.
- O'Connor, K.M. and Dowding, C.H. (1999), *Geomeasurements by pulsing TDR cables and probes*, CRC Press.
- Selker, J.S., Graff, L. and Steenhuis, T. (1993), “Noninvasive time domain reflectometry moisture measurement probe”, *Soil. Sci. Soc. Am. J.*, **57**(4), 934-936.
- Siddiqui, S.I. and Drnevich, V. P. (1995), *Use of Time Domain Reflectometry for Determination of Water Content and Density of Soil*, Technical Report.
- Su, M.B. and Chen, Y.J. (1998), “Multiple reflection of metallic time domain reflectometry”, *Exper. Tech.*, **22**(1), 26-29.
- Topp, G.C. and Davis, J.L. (1985), “Measurement of Soil Water Content Using Time Domain Reflectometry (TDR): A Field Evaluation”, *Soil. Sci. Soc. Am. J.*, **49**(3), 35-39.
- Vaz, C.M.P. and Hopmans, J.W. (2001), “Simultaneous measurement of soil penetration resistance and water content with a combined penetrometer–TDR moisture probe”, *Soil. Sci. Soc. Am. J.*, **65**(1), 4-12.
- White, I. and Zegelin, S.J. (1994), “Comments on ‘Considerations on the use of time-domain reflectometry (TDR) for measuring soil water content’ by WR Whalley”, *Eur. J. Soil. Sci.*, **45**(4), 503-508.
- Yu, X. (2009), *Experimental Study of an Innovative Bridge Scour Sensor*, Ph.D. Dissertation, Case Western Reserve University.
- Yu, X. and Drnevich, V.P. (2004), “Soil water content and dry density by time domain reflectometry”, *J.*

Geotech. Geoenviron., **130**(9), 922-934.

Yu, X. and Yu, X. (2009), "Time domain reflectometry automatic bridge scour measurement system: principles and potentials", *Struct. Health Monit.*, **8**(6), 463-476.

BS